ORIGINAL RESEARCH

Naodesheng Pills Ameliorate Cerebral Ischemia Reperfusion-Induced Ferroptosis via Inhibition of the ERK1/2 Signaling Pathway

Yong-Yu Yang [1,2], Rong-Rong Deng[3], Da-Xiong Xiang[1,2]

[1]Department of Pharmacy, The Second Xiangya Hospital of Central South University, Changsha, Hunan, People's Republic of China; [2]Hunan Provincial Engineering Research Central of Translational Medical and Innovative Drug, The Second Xiangya Hospital of Central South University, Changsha, Hunan, People's Republic of China; [3]School of Traditional Chinese Medicine, Guangdong Pharmaceutical University, Guangzhou, Guangdong, People's Republic of China

Correspondence: Yong-Yu Yang; Da-Xiong Xiang, Department of Pharmacy, The Second Xiangya Hospital, Central South University, 139#, Renmin Middle Road, Changsha, Hunan, 410011, People's Republic of China, Tel/Fax +86-731-85292129, Email yongyuyang@csu.edu.cn; xiangdaxiong@csu.edu.cn

Background: Ferroptosis plays a crucial role in the occurrence and development of cerebral ischemia-reperfusion (I/R) injury and is regulated by mitogen-activated protein kinase 1/2 (ERK1/2). In China, Naodesheng Pills (NDSP) are prescribed to prevent and treat cerebrosclerosis and stroke. However, the protective effects and mechanism of action of NDSP against cerebral I/R-induced ferroptosis remain unclear. We investigated whether NDSP exerts its protective effects against I/R injury by regulating ferroptosis and aimed to elucidate the underlying mechanisms.

Methods: The efficacy of NDSP was evaluated using a Sprague-Dawley rat model of middle cerebral artery occlusion and an in vitro oxygen-glucose deprivation/reoxygenation (OGD/R) model. Brain injury was assessed using 2,3,5-triphenyltetrazolium chloride (TTC), hematoxylin and eosin staining, Nissl staining, and neurological scoring. Western blotting was performed to determine the expression levels of glutathione peroxidase 4 (GPX4), divalent metal-ion transporter-1 (DMT1), solute carrier family 7 member 11 (SLC7A11), and transferrin receptor 1 (TFR1). Iron levels, oxidative stress, and mitochondrial morphology were also evaluated. Network pharmacology was used to assess the associated mechanisms.

Results: NDSP (1.08 g/kg) significantly improved cerebral infarct area, cerebral water content, neurological scores, and cerebral tissue damage. Furthermore, NDSP inhibited I/R- and OGD/R-induced ferroptosis, as evidenced by the increased protein expression of GPX4 and SLC7A11, suppression of TFR1 and DMT1, and an overall reduction in oxidative stress and Fe^{2+} levels. The protective effects of NDSP in vitro were abolished by the GPX4 inhibitor RSL3. Network pharmacology analysis revealed that ERK1/2 was the core target gene and that NDSP reduced the amount of phosphorylated ERK1/2.

Conclusion: NDSP exerts its protective effects against I/R by inhibiting cerebral I/R-induced ferroptosis, and this mechanism is associated with the regulation of ferroptosis via the ERK1/2 signaling pathway.

Keywords: Naodesheng pills, ferroptosis, cerebral ischemia/reperfusion, glutathione peroxidase 4, mitogen-activated protein kinase 1/2

Introduction

Stroke is widely recognized as a major disease that leads to death and disability in patients globally.[1] Each year, approximately 2.4 million people suffer a stroke episode, with an estimated 1.1 million fatalities, consequently imposing a heavy burden on patients' families and society.[2] There are three primary types of strokes: ischemic, hemorrhagic, and transient. Ischemic stroke occurs when blood flow to the brain is obstructed by thrombosis or embolism and accounts for 87% of all strokes.[3] Timely restoration of blood supply to the ischemic cerebral tissue by thrombolysis or mechanical recanalization of blood vessels is currently the optimal treatment for improving the prognosis of ischemic stroke.[4] However, in several cases, the restoration of blood supply to ischemic tissue may exacerbate the brain injury, a condition known as "ischemia-reperfusion" (I/R) injury.[5] Therefore, identifying an effective method to reduce the incidence of I/R injury is essential for treating ischemic stroke.

Ferroptosis is a distinct form of programmed cell death that differs from apoptosis, necrosis, and autophagy.[6] It is characterized by the iron-dependent accumulation of lipid peroxides and is associated with various neurological pathologies, including cerebral I/R injury, Alzheimer's disease, and Parkinson's disease.[7,8] Ferroptosis is typically regulated by the solute carrier family 7 member 11 (SLC7A11)/glutathione peroxidase 4 (GPX4) pathway, iron metabolism (transferrin receptor [TFR1]/divalent metal ion transporter-1 [DMT1] pathway), and lipid peroxidation.[9] Iron chelation or restoration of GPX4 expression has been shown to attenuate I/R-induced brain injury.[10,11] The mitogen-activated protein kinase (MAPK)/extracellular signal-regulated kinase (ERK1/2) was reported to be activated and involved in cerebral I/R injury,[12] and the inhibition of the ERK1/2 pathway reduces middle cerebral artery occlusion-induced infarct size.[13] ERK1/2 plays a crucial role in modulating ferroptosis[14] and the inhibition of ERK1/2 signaling has been reported to be essential for preventing ferroptosis.[15] Therefore, inhibiting ERK1/2-mediated ferroptosis may be an effective strategy for preventing or treating cerebral I/R injury.

Naodesheng pills (NDSP) are commonly prescribed traditional Chinese medicines consisting of *Panax notoginseng* (Burk.) F. H. Chen, *Carthamus tinctorius* L., *Crataegus pinnatifida* Bunge and *Pueraria lobata* (Willd.). Ohwi, and *Ligusticum chuanxiong* Hort.[16] The major bioactive components of NDSP have been reported to include flavones (puerarin and daidzein), saponins (ginsenosides Rg1, Rg2, Rb1, Rd, Rh1, and notoginsenoside R1), and phenylpropanoids (Safflower yellow A and ferulic acid).[16–18] In clinical practice, NDSP has been used to treat ischemic stroke and cerebral hemorrhage.[19] Animal experiments have shown that naodesheng (NDS) improves learning and memory function by inhibiting NF-κB and activation of cAMP/PKA/CREB signaling pathway in amyloid β-treated rats.[20] The main components of NDSP, such as tetramethyl pyrazine,[21] hydroxysafflor yellow A,[22] and puerarin,[23] could promote the recovery of neurological function after stroke. However, the therapeutic effects of NDS on ischemic brain injury have been inconsistent. In the FeCl$_3$-induced focal cerebral ischemic model, NDS improved the neurological deficit score and cerebral infarction.[24] Li et al found that, after 26h of administration, NDS showed a decreasing trend in infarct size and neurological deficit score in a model of permanent cerebral ischemia.[25] Seven days after administration, NDS significantly improved ischemia-induced nerve damage and superoxide dismutase.[25] Further studies are required to evaluate the effects of NDSP on I/R-induced cerebral injury. Although recent metabolomic investigations have revealed that NDSP affects multiple metabolic pathways, such as energy and amino acid metabolism, oxidative stress, and inflammatory pathways,[26] the therapeutic mechanism remains unclear. As the components of NDSP inhibit ERK1/2 activation[27–29] and ferroptosis,[30–32] we hypothesized that NDSP exerts a neuroprotective effect against I/R injury by regulating ferroptosis. Therefore, in this study, we investigated effects of NDSP and its mechanism of action on ferroptosis, both in vitro and in vivo.

Materials and Methods
Materials
NDSP was obtained from Hunan TianJi CaoTang Pharmaceutical Co., Ltd. (Changsha, China) and comprised *Panax notoginseng* (Burk.) F. H. Chen (11.73%), *Carthamus tinctorius* L. (13.68%), *Crataegus pinnatifida* Bunge (23.61%), *Pueraria lobata* (Willd.) Ohwi (39.25%), and *Ligusticum chuanxiong* Hort (11.73%). CoCl$_2$ was purchased from the Aladdin Company, Ltd. (Shanghai, China). Anti-SLC7A11 and iron assay kits were purchased from Abcam (Cambridge, UK). Anti-β-actin antibody was purchased by Boster Biological Technology Co., Ltd. (Wuhan, China) or Servicebio (Wuhan, China). Anti-DMT1 and secondary antibodies were purchased from Boster Biological Technology Co. Ltd. (Wuhan, China). The anti-ERK1/2 antibody was purchased from Proteintech (Wuhan, China), and anti-phosphorylated ERK1-T202/Y204+ERK2-T185/Y187 antibodies were purchased from Abclonal (Wuhan, China). Anti-TFR1 antibodies were obtained from Affinity Biosciences (Jiangsu, China). In contrast, anti-GPX4 antibodies, superoxide dismutase (SOD), glutathione (GSH), hydrogen peroxide (H$_2$O$_2$), malondialdehyde (MDA), DCFH-DA, and Hoechst 33342/PI assay kits were purchased from the Beyotime Institute of Biotechnology (Jiangsu, China). The RSL3 was acquired from Selleck Co., Ltd. (Shanghai, China). A hematoxylin and eosin (H&E) staining kit, Nissl staining solution, and triphenyl tetrazolium chloride (TTC) solution (2%) were purchased from Solarbio Co., Ltd. (Beijing, China). Dulbecco's Modified

Eagle's medium (DMEM) and fetal bovine serum (FBS) were purchased from HyClone Laboratories, Inc. (Logan, UT, USA).

Animals

Male Sprague-Dawley rats aged eight weeks (200–250 g) were purchased from SiLaike JingDa (Changsha, China) and housed in cages with standard food and water provided ad libitum. All experimental protocols were designed according to the Guide for the Care and Use of Laboratory Animals (NIH Publication, 8th edition, 2011) and approved by the Animal Ethics and Welfare Committee of the Second Xiangya Hospital of Central South University (No. 2021955).

Drug Treatment and Focal Cerebral I/R Rat Model

The Resource Equation Method was used to estimate the sample size of animal experiments.[33] According to the formula, $n = 10/k + 1$ (k = number of groups, n = number of subjects per group), the minimum number of animals in each group is three rats, and the total sample size is at least 18 rats. In order to obtain sufficient experimental data, a total of 48 rats were used for the experiments and randomly divided into six groups of eight individuals each: control, sham, I/R, low-dose NDSP (NDSP-L), high-dose NDSP (NDSP-H), and edaravone group (positive control). The daily dose of NDSP administered to adults weighing 60 kg was 6 g. According to the body surface area method, the equivalent dose for rats was 0.54 g/kg. This dose was used as the low-dose group in this experiment, and twice the dose was employed as the high-dose group. The NDSP was dissolved in 0.25% CMC-Na and intragastrically administered at doses of 0.54 g/kg or 1.08 g/kg once daily for seven days. The rats in the I/R, normal control, and sham groups were administered equal volumes of CMC-Na. After seven days of drug treatment, rats in the I/R, NDSP-L, edaravone, and NDSP-H groups were subjected to I/R. A rat cerebral I/R model was established.[34] Briefly, the rats were anesthetized with an intraperitoneal injection of 2% pentobarbital sodium (30 mg/kg), and a midline incision was made in the neck. The left common carotid artery (CCA), external carotid artery (ECA), and internal carotid artery (ICA) were isolated. The CCA and ECA were ligated, and the ICA was temporarily clipped using an artery clamp. A nylon suture was then inserted externally into the ECA. After blocking the blood flow for 2 h, reperfusion was performed for 24 h. Rats in the sham group underwent the same procedure without nylon suture insertion.

Assessment of Neurological Function

Neurological deficits were assessed based on a five-point neurological deficit score, as previously described[35] (0 = no observable symptoms of neurological deficits, 1 = failure of fully extending the right forepaw, 2 = circling to the right, 3 = falling to the right, 4 = unable to walk spontaneously, and loss of consciousness). Scoring was performed independently by two researchers who were blinded to the experimental groups.

Assessment of Cerebral Infarct Area

After 24h of I/R, the rats were injected intraperitoneally with 2% sodium pentobarbital (150 mg/kg) and sacrificed by decapitation. Infarct area following cerebral I/R injury in rats was determined by 2,3,5-triphenyltetrazolium chloride (TTC) staining. The brain was removed quickly and cut into five 2-mm slices using a rat brain fixator and blade. The sections were incubated with 2% TTC for 25 min at 37 °C and fixed in 4% formaldehyde solution for 24 h. Next, the slices were captured as a digital image and analyzed using ImageJ software (1.37c). The infarct area ratio (%) was calculated as follows:

$$\text{Infarct area}\,(\%) = \text{infarct area}/\text{total cross} - \text{sectional area} \times 100\%$$

Assessment of Cerebral Water Content

Following I/R, the brain tissues were weighed before being placed in a constant-temperature drying oven at 110 °C for 48 h. The dry brain tissue was weighed again, and the cerebral water content was calculated as follows:

$$\text{Cerebral water content}\,(\%) = (\text{wet mass} - \text{dry mass})/\text{wet mass} \times 100\%$$

Histopathological Evaluation

Rat brain tissue was fixed in 4% paraformaldehyde. Then, the tissue block was dehydrated in 70%, 80%, 90%, and 95% ethanol for 10 min each, embedded in paraffin, and sliced into five μm-thick slices. The slices were deparaffinized and stained with hematoxylin, eosin, or Nissl stain to observe histological changes.

Immunohistochemistry

The sections were then deparaffinized and rehydrated. Following antigen retrieval, the sections were treated with 3% H_2O_2 to block endogenous peroxidase activity and were subsequently blocked with 3% sheep serum at 37 °C for 1 h. Then, sections were incubated with the primary anti-p-ERK1/2 antibody at 4 °C overnight. After washing with PBS, the sections were incubated with HRP-conjugated secondary antibodies and stained with DAB, followed by hematoxylin counterstaining. The stained sections were observed under a light microscope.

Biochemical Analysis

The levels of MDA, GSH, H_2O_2, SOD, released lactate dehydrogenase (LDH), and iron in the cerebral tissue or SH-SY5Y cells were determined according to the manufacturer's instructions.

Western Blot Analysis

Total protein from the brain tissue or SH-SY5Y cells was extracted in RIPA lysis buffer (Beyotime, P0013C), and the protein concentration was quantified using a BCA kit (Beyotime, P0010S). SDS-PAGE (10%) separated forty micrograms of protein from each sample; the samples were subsequently transferred from the gel to a nitrocellulose membrane. Membranes were blocked for 1 h with 5% skimmed milk at room temperature, followed by incubation with GPX4 (1:500), SLC7A11 (1:250), TFR1 (1:500), DMT1 (1:500), ERK1/2 (1:500), and p-ERK1/2 (1:500) at 4 °C overnight. The membrane was washed three times in TBST buffer and incubated with secondary antibodies at room temperature for 1 h. Blots were developed using enhanced chemiluminescence reagents. Band intensity was employed as a readout for the relative expression level of each target protein, and this was normalized to the expression of β-actin in each sample.

Cell Culture and the Oxygen-Glucose Deprivation Model

The SH-SY5Y cells were provided by the Chinese Academy of Sciences (Shanghai, China) and were cultured in DMEM supplemented with 10% (v/v) FBS at 37 °C and 5% CO_2. An oxygen-glucose deprivation/reperfusion (OGD/R) model was established to mimic I/R injury.[36] SH-SY5Y cells were incubated in glucose- and serum-free DMEM containing $CoCl_2$ (400 μM) for 6 h to simulate ischemia. The culture medium was then replaced with fresh DMEM supplemented with 10% fetal bovine serum (FBS) for 24 h to represent reperfusion. Control cells were incubated in DMEM supplemented with 10% FBS throughout the whole process.

Assessment of Cell Viability

The MTT assay measured the effect of NDSP on SH-SY5Y cellular viability. Briefly, SH-SY5Y cells were grown in a 96-well plate and divided into the control and NDSP groups. NDSP was dissolved in PBS. The cells in the NDSP group were treated with varying concentrations of NDSP (6.25, 12.5, 25, 50, and 100 μg/mL) for 24 h. Cells in the control group were treated with the same volume of PBS. Next, the cells in each well were incubated with MTT (5 mg/mL) at 37 °C for 3 h. Formazan was dissolved in DMSO, and the optical density (OD) value was determined at 570 nm using a microplate reader. Cell viability was calculated as the percentage of the OD value relative to that of the control group (representing 100% viability).

To evaluate the protective effect of NDSP against OGD/R-induced cell injury, the cells were divided into control, OGD/R, and NDSP groups. The cells in the NDSP group were pre-incubated with different concentrations of NDSP (3.125, 6.25, 12.5, and 25 μg/mL) for 6 h. OGD/R and NDSP cells were subjected to OGD/R. Afterward, the cell viability was measured by the MTT assay.

Hoechst 33342-PI Staining

The cell death was detected using Hoechst 33342/PI following the manufacturer's protocol. Briefly, cells were divided into control, NDSP, OGD/R, and +NDSP groups. Cells in the NDSP and +NDSP groups were pretreated with NDSP (6.25 μg/mL) for 6 h. Cells in the OGD/R and +NDSP groups were subjected to OGD/R. After treatment, the culture medium was removed, and the cells were incubated with a working Hoechst 33342/PI solution for 30 min in the dark at 37°C. The fluorescence intensity of each well was recorded using a fluorescence microscope (Zeiss AG, Oberkochen, Germany).

DCFH-DA Staining

Reactive oxygen species (ROS) were detected using a DCFH-DA assay kit following the manufacturer's protocol. Briefly, the cells were divided into the control, OGD/R, OGD/R+NDSP, and OGD/R+NDSP+RSL3 group. Cells in the OGD/R+NDSP+RSL3 group were preincubated with NDSP (6.25 μg/mL) and RSL3 (30 nM) for 6 h. Cells in the OGD/R+NDSP group were pre-incubated with NDSP for 6 h. Cells in the control and OGD/R groups were treated with the same volume of DMSO (0.1%) for 6 h. Cells in the OGD/R+NDSP and OGD/R+NDSP+RSL3 groups were subjected to OGD/R. After cell treatment, the culture medium was removed, and the cells were incubated with a working solution of DCFH-DA for 30 min in the dark at room temperature. The fluorescence intensity of each well was recorded using a fluorescence microscope (Zeiss AG, Oberkochen, Germany).

Transmission Electron Microscopy

The SH-SY5Y Cells were fixed in 4% glutaraldehyde and 1% osmic tetroxide at 4 °C. The cells were then dehydrated with 50%, 70%, 80%, and 90% ethanol for 15 min each, followed by dehydration with 100% ethanol three times for 30 min each, and embedded in Eponate 12 resin. Ultrathin sections (50–70 nm thick) were obtained and stained with uranyl acetate and lead citrate solutions for transmission electron microscopy (TEM). Images were captured using a JEOL 1200EX-II electron microscope (Akishima, Japan).

Screening for Active Ingredients and Targets in NDSP

The candidate ingredients of NDSP (*Panax notoginseng* [Burk] F.H. Chen, *Carthamus tinctorius* L., *Crataegus pinnatifida* Bunge, *Pueraria lobata* [Willd.] Ohwi, and *Ligusticum chuanxiong* Hort) were obtained from the Traditional Chinese Medicine Systems Pharmacology Database and Analysis Platform (TCMSP, (http://tcmspw.com/tcmsp.php), Encyclopedia of Traditional Chinese Medicine (ETCM; http://www.tcmip.cn/ETCM/index.php), and Batman databases. The candidate compounds were first screened through the TCMSP database, using the following screening criteria: Oral bioavailability ≥ 30% and Drug Likeness ≥ 0.18. If no absorption, distribution, metabolism, or excretion (ADME) parameters existed for the candidate compound in the TCMSP database, we used the Swiss ADME database to obtain the compound's ADME parameters. The screening criteria met the requirements for the gastro-intestinal absorption GIabsort to be "High" and with at least two "Yes" hits in Drug Likeness (Lipinski, Ghose, Veber, Egan, Muegge). In addition, based on literature reports, puerarin, ursolic acid, hydroxy safflower yellow A, and notoginseng saponin R1 are potential supplementary active ingredients of NDSP. Targets of the active compounds were obtained from the Swiss TargetPrediction database; targets with scores greater than 0 were classified as possible targets.

Collection of Disease-Related Targets

Disease targets were obtained from the OMIM (https://omim.org/), Genecards (http://www.genecards.org/), Drugbank (https://www.drugbank.com), and TTD databases (http://db.idrblab.net/ttd/) using the terms "cerebral ischemia-reperfusion injury" and "ischemic stroke".

Drug-Ingredient-Disease-Target Network Construction and Vital Active Ingredients Analysis

Common targets of the drugs and diseases were identified using Venny2.1 (https://bioinfogp.cnb.csic.es/tools/). The Drug-Ingredient-Disease-Target network was constructed using Cytoscape 3.9.2. The key active ingredients were determined using a NetworkAnalyzer. The degree value represents the number of links between ingredients and their targets. The higher the degree value, the more critical the component.

Protein-Protein Interaction Network Construction and Core Target Analysis

The protein-protein interaction (PPI) network of common targets was constructed using the STRING database (https://string-db.org/), with the species limited to "Homo sapiens" and a minimum interaction threshold of 0.9. At the same time, the PPI network interaction data was obtained, and the topology analysis of the common targets was carried out using the NetworkAnalyzer of Cytoscape 3.9.2 software. The top 20 targets were selected based on the degree value, and the core target diagram was drawn using R 4.2.1.

GO Enrichment and KEGG Pathway Analysis

GO enrichment analysis and KEGG pathway annotation of common targets were performed using the online tool DAVID (https://david.ncifcrf.gov).

Molecular Docking

The top six compounds were selected for molecular docking analysis with ERK1 or ERK2 based on the degree values. The predicted structures of the active ingredients were downloaded from PubChem (https://pubchem.ncbi.nlm.nih.gov/), and those of the target proteins were downloaded from the Protein Data Bank database (https://www.rcsb.org/). The Schrödinger Maestro software was used to perform molecular docking, and the binding activity of the target protein to the compound was ranked based on the docking score. Discovery Studio 3.6 software was used to visualize the docking results and identify the binding residues. Molecular dynamics simulations were performed with AMBER 18 program.

Statistical Analysis

All data are expressed as the mean ± standard error of the mean (SEM), and data were analyzed using SPSS 29.0 software or GraphPad Prism 7.03. For $n \geq 5$, use the Q-Q plot and Levene's test to test the normality and homogeneity of variance of the data, respectively. If the data showed normality and equal variation, the significance of the difference between multiple groups was analyzed by one-way analysis of variance (ANOVA) followed by Tukey's post-hoc test. If the data showed non-normal distribution or biased variation, statistical significance was analyzed by Kruskal Wallis test with a two-stage linear step-up procedure from the Benjamini, Krieger, and Yekutieli test for multiple comparisons using GraphPad Prism. For n=3, the bootstrap method was used to analyze the data. A P-value < 0.05 was considered statistically significant.

Results

NDSP Attenuates OGD/R-Induced Ferroptosis in SH-SY5Y Cells

The SH-SY5Y cells were exposed to different concentrations of NDSP (6.25, 12.5, 25, 50, and 100 μg/mL) for 24 h. We observed that NDSP did not exert any toxic effects on SH-SY5Y cells at concentrations below 100 μg/mL (Figure 1A). To evaluate the protective effects of NDSP against cell death, an in vitro $CoCl_2$-induced OGD/R model was established. As depicted in Figure 1B, treatment with NDSP (6.25–25 ng/mL) significantly enhanced cell viability compared to that in the OGD/R group. Moreover, SH-SY5Y cells treated with NDSP (6.25 μg/mL) exhibited an inhibition of OGD/R-induced cell death ($P=0.039$) (Figure 1C) along with increased levels of Fe^{2+} ($P=0.035$) and MDA ($P=0.038$) (Figure 1D and E). Additionally, treating SH-SY5Y cells with NDSP mitigated the decline in GPX4 expression ($P=0.011$) mediated by OGD/R and promoted the expression of TFR1 ($P=0.032$) and DMT1 ($P=0.043$) (Figure 1F).
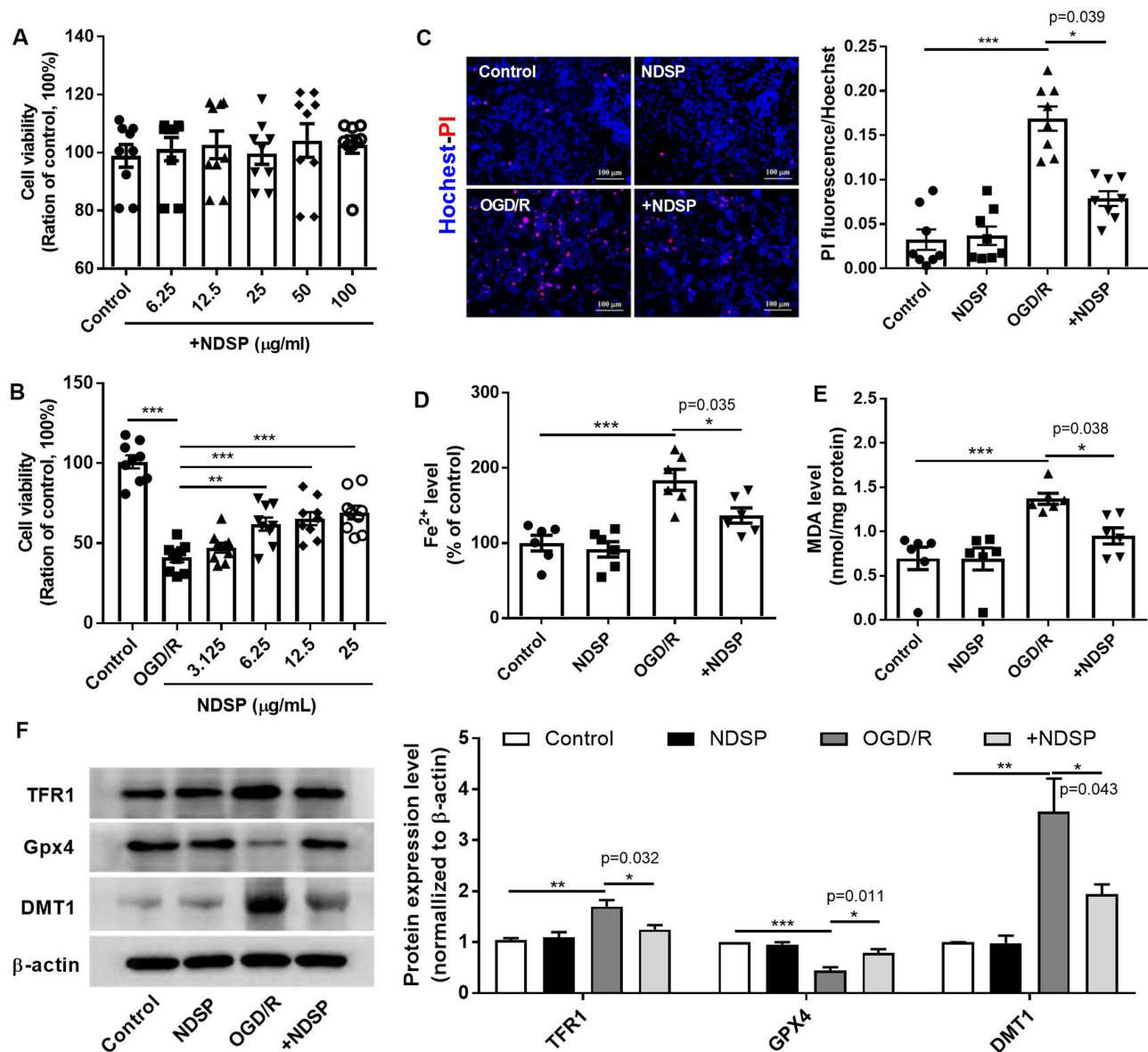
Figure 1 NDSP attenuates ferroptosis in vitro. (**A**) The effect of different concentrations of NDSP on cell viability. (**B**) The effect of NDSP on OGD/R-induced cell injury. (**C**) Hoechst-PI staining (200× magnification, scale bar: 100 μm). (**D**) Fe^{2+} level. (**E**) MDA level. (**F**) Western blot analysis of TFR1, GPX4, and DMT1 protein levels. The β-actin was used as the loading control. Data presented as mean ± SEM (n ≥ 3 independent experiments; statistical analysis performed by SPSS 29.0 software or GraphPad Prism (version 7.03); *$P < 0.05$, **$P < 0.01$, ***$P < 0.001$).
Abbreviations: NDSP, Naodesheng pills; OGD/R, Oxygen-glucose deprivation/ reoxygenation.

NDSP Reduces OGD/R-Induced Cell Injury via Ferroptosis

RSL3 is an inhibitor of GPX4 as it sequesters and inactivates the enzyme, thereby promoting ferroptosis.[37] Incubation with RSL3 (30 nM) abolished the protective effects of NDSP against the OGD/R-induced decline in cell viability (P=0.001) (Figure 2A) and LDH release (P=0.002) (Figure 2B). Similarly, the NDSP-treated group showed down-regulated levels of MDA and ROS, accompanied by the upregulation of GSH.

The protective effects of NDSP were negated when the cells were treated with RSL3 (P<0.001) (Figure 2C–F). Regarding morphological changes, TEM analysis revealed that NDSP treatment attenuated mitochondrial swelling and reduced mitochondrial density in SH-SY5Y cells; however, co-incubation with RSL3 abolished these changes (Figure 2G). Collectively, these results indicated that NDSP effectively inhibited OGD/R-induced ferroptosis in vitro.
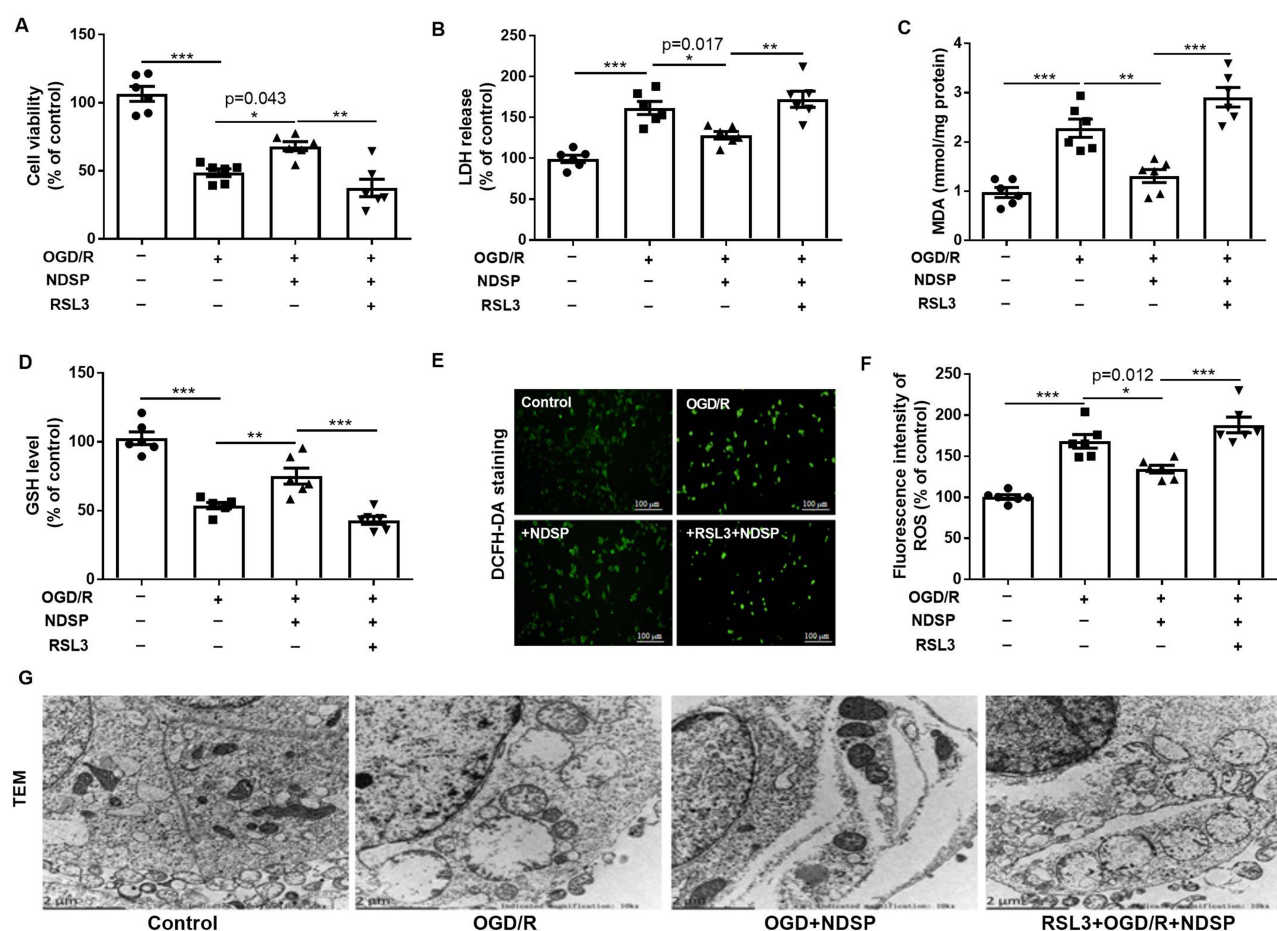
Figure 2 NDSP reduces OGD/R-induced cell injury by regulating ferroptosis. (**A**) Cell viability. (**B**) LDH levels in the cell culture supernatant. (**C**) MDA levels. (**D**) GSH levels. (**E**) DCFH-DA staining (200× magnification, scale bar: 100 μm). (**F**) Fluorescence intensity of ROS. (**G**) Representative transmission electron microscopy images of SH-SY5Y cells (10,000× magnification, scale bar: 2 μm). Data presented as mean ± SEM (n ≥ 3 independent experiments; statistical analysis performed by SPSS 29.0 software or GraphPad Prism (version 7.03); *$P < 0.05$, **$P < 0.01$, ***$P < 0.001$).
Abbreviations: NDSP, Naodesheng pills; OGD/R, Oxygen-glucose deprivation/reoxygenation.

NDSP Decreases I/R-Induced Cerebral Injury in vivo

There was no significant difference in the infarct area between the sham and control groups. However, the infarct area, neurological score, and cerebral water content in the I/R-treated rats were significantly higher than in the sham group ($P<0.001$). Rats treated with NDSP-H exhibited smaller cerebral infarct area, reduced neurological damage, and lower cerebral water content than the rats in the I/R group ($P=0.007$, $P=0.025$, and $P<0.001$) (Figure 3A–D). Histological examination of these rats' cerebral cortex and hippocampus revealed that NDSP attenuated the shrunken and pyknotic nuclei and the swollen tissue induced by I/R, as depicted in Figure 3E. In addition, Nissl staining showed fewer Nissl bodies in the I/R group than in the sham group. However, NDSP-H-treated rats had higher Nissl body than the I/R group (Figure 3F). These data suggested that NDSP reduced cerebral I/R injury.

NDSP Alleviates Cerebral I/R-Induced Ferroptosis

Figure 4A–C demonstrates that NDSP administration in rats significantly inhibited the I/R-induced increases in MDA, H_2O_2, and Fe^{2+} levels ($P<0.001$, $P=0.018$, and $P=0.005$). Furthermore, although the protein levels of GSH and SOD decreased following I/R, they were elevated in rats treated with NDSP relative to those in the I/R group ($P=0.034$ and $P=0.002$) (Figure 4D and E). Western blot analysis revealed that NDSP-treated rats exhibited higher protein levels of SLC7A11 and GPX4 ($P=0.003$ and $P=0.028$) and lower protein expression of TFR1 and DMT1 ($P=0.049$ and $P=0.025$)
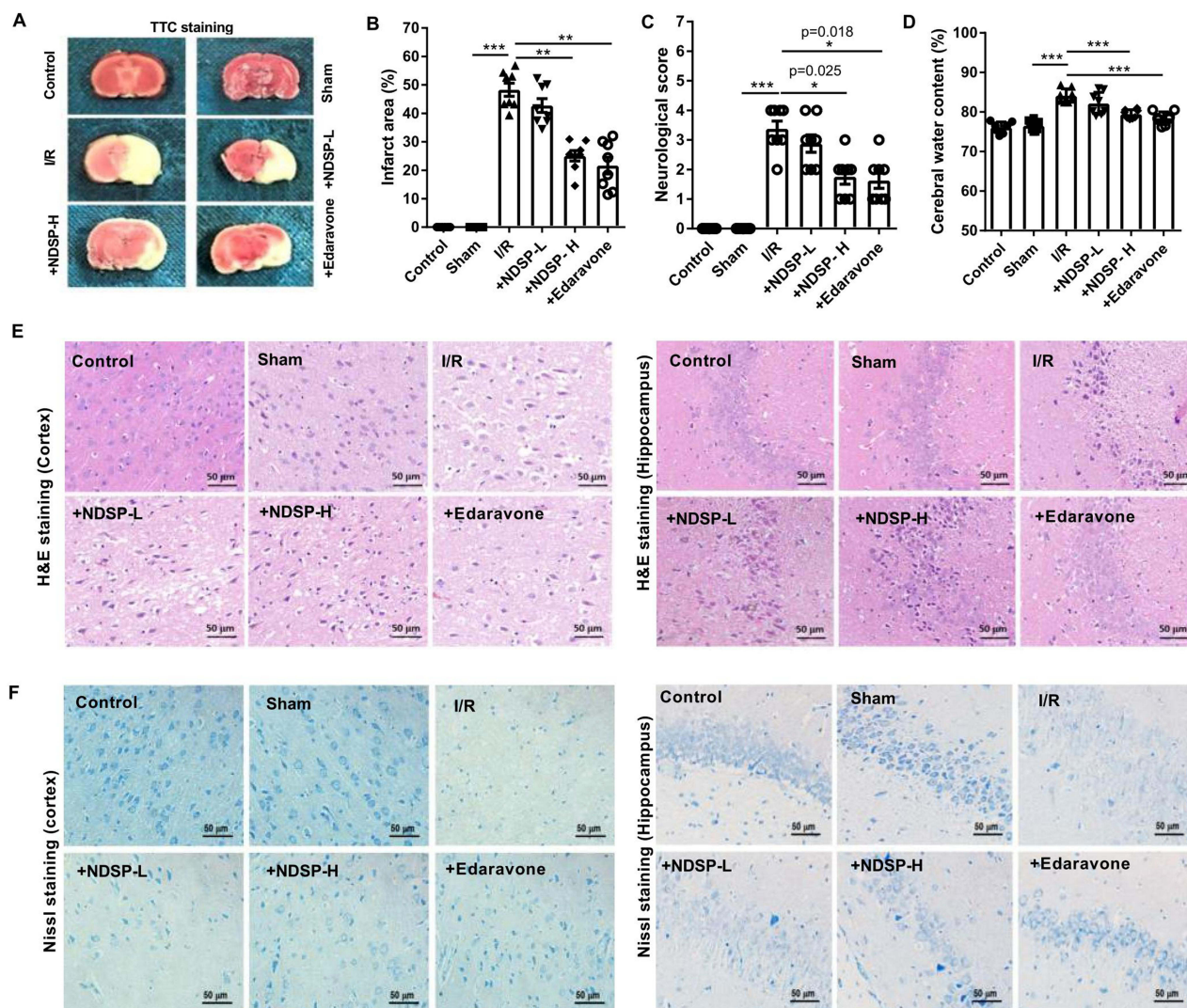
Figure 3 NDSP decreases I/R-induced cerebral injury in vivo. (**A**) Representative images of TTC-stained rat brain tissue. (**B**) Infarct area of each treatment group. (**C**) Neurological deficit scores in each treatment group. (**D**) Cerebral water content. (**E**) Representative images of H&E staining (400× magnification, scale bar: 50 μm). (**F**) Representative images of Nissl staining (400× magnification, scale bar: 50 μm). Data presented as mean ± SEM (n = 8; statistical analysis performed by SPSS 29.0 software or GraphPad Prism (version 7.03); *$P < 0.05$, **$P < 0.01$, ***$P < 0.001$).
Abbreviations: I/R, Ischemia-reperfusion; NDSP, Naodesheng pills; NDSP-L, low-dose NDSP; NDSP-H, high-dose NDSP.

than I/R-treated rats (Figure 4F and G). These findings suggest that NDSP mitigates I/R-induced ferroptosis in the cerebral tissue.

Ferroptosis-Regulating Genes as Candidate Targets of NDSP Activity

We employed a computational approach based on network pharmacology to delineate further the mechanism of action of NDSP in cerebral I/R-mediated ferroptosis. Some 135 active ingredients were identified (Supplementary Table S1), and 1042 drug targets were selected from the Swiss TargetPrediction database (Supplementary Table S2). Furthermore, 669 disease-related genes were included in the I/R dataset (termed "disease dataset"), after querying the OMIM, Genecards, DrugBbank, and TTD databases (Supplementary Table S3). Next, we constructed an overlapping set of 203 common targets whose expression was affected by either NDSP or I/R (Supplementary Table S4). The percentages of targets in the NDSP, I/R, and their overlapping set are shown in Figure 5A. The Drug-Ingredient-Disease-Target dataset used 135 potential active ingredients and 203 common drug-disease targets (Figure 5B). Our analysis of the key active ingredients showed that officinalic acid, baicalein, cnidium lactone, senkyunone, lignan, and (-)-dicentrine were the top candidates
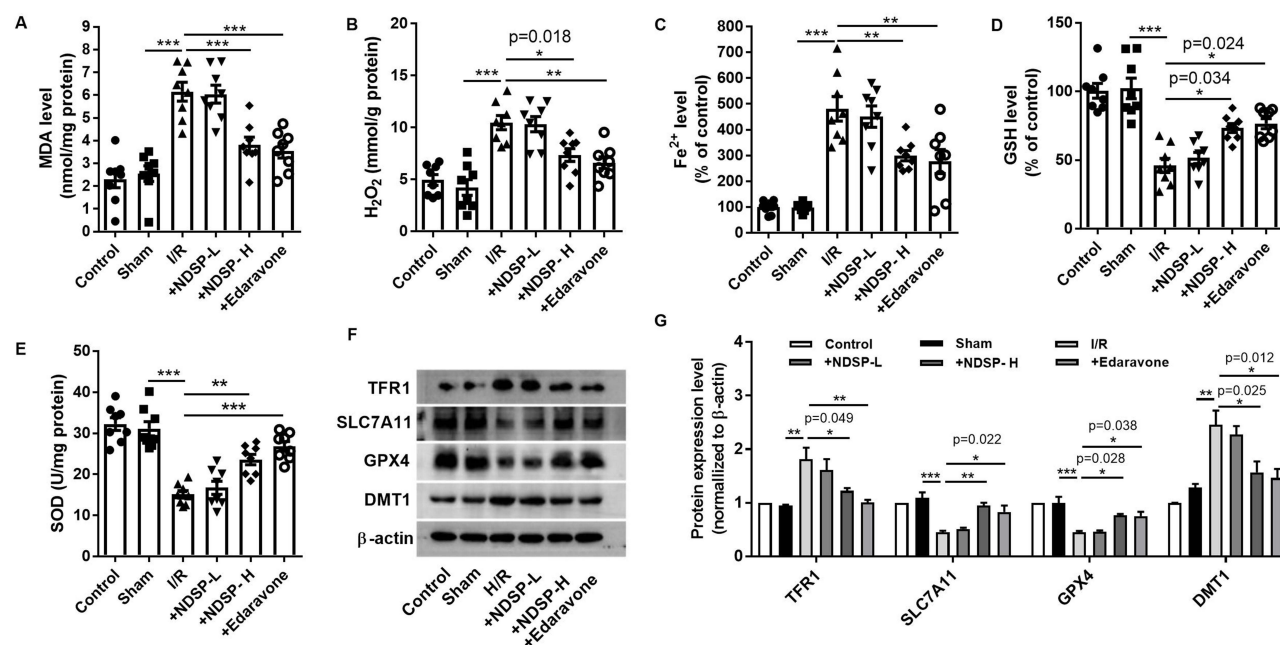
Figure 4 NDSP alleviates I/R-induced ferroptosis in rat cerebra. (**A**) MDA levels. (**B**) H_2O_2 levels. (**C**) Fe^{2+} levels. (**D**) GSH levels. (**E**) SOD levels. (**F**) Western blot analysis of TFR1, SLC7A11, GPX4, DMT1 protein levels. The β-actin was used as the loading control. (**G**) Densitometric analyses of TFR1, SLC7A11, GPX4, and DMT1. Data presented as mean ± SEM (n ≥ 3; statistical analysis performed by SPSS 29.0 software or GraphPad Prism (version 7.03); *$P < 0.05$, **$P < 0.01$, ***$P < 0.001$).
Abbreviations: I/R, Ischemia-reperfusion; NDSP, Naodesheng pills; NDSP-L, low-dose NDSP; NDSP-H, high-dose NDSP.

that may be primarily responsible for the protective effects of NDSP (Supplementary Table S5). Results of GO-biological process analysis of 203 common targets indicated that the targets of NDSP mainly included "response to a drug", "response to hypoxia", "inflammatory response", and "positive regulation of the ERK1 and ERK2 cascade". Cellular components include the plasma membrane, cell surface, and membrane rafts. Molecular functions were predominantly related to identical proteins, enzymes, and protein binding (Figure 5C). The results of the KEGG enrichment analysis indicated that lipids and atherosclerosis, the MAPK signaling pathway, and the hypoxia-inducible factor signaling pathway may mediate the effects of NDSP in NDSP-regulated cerebral injury (Figure 5D).

NDSP Regulates Ferroptosis via ERK1/2

A PPI network comprising 203 common targets was constructed (Figure 6A). According to the topological analysis of the constructed PPI network, the top 20 core targets ranked according to the *P*-values are shown in Supplementary Table S6. *MAPK3, SRC, MAPK1, STAT3, TP53, AKT1, JUN, NFKB1, MAPK14,* and *PIK3CA* were the top ten core targets implicated in the effects of NDSP (Figure 6B). Among these, *ERK1/2* (MAPK3 and MAPK1) emerged as crucial genes involved in ferroptosis regulation and served as a core target, ranking first and third in the network pharmacology approach. Therefore, we investigated the effects of NDSP on the expression of ERK1/2. As shown in Figure 6C, NDSP markedly reduced the ratio of phosphorylated ERK1/2 (p-ERK1/2) to total ERK1/2 in SH-SY5Y cells exposed to OGD/R (*P*=0.019). Similarly, immunohistochemical staining of the rat brain tissue sections demonstrated that NDSP-H treatment attenuated the increased expression of p-ERK1/2 after I/R injury (Figure 6D). To further explore the molecular interactions, we performed molecular docking of the six most important active ingredients, namely, officinalic acid, baicalein, cnidium lactone, senkyunone, lignan, and (-)-dicentrine, with ERK1 and ERK2. These results indicate that baicalein exhibits a strong binding affinity for ERK1 and ERK2. Several residues, including LYS-52 and Glu-69 of ERK2 and Asp-123 and Met-125 of ERK1, formed hydrogen bonds with baicalein (Figure 6E). The binding score are presented in Supplementary Table S7. Next, molecular dynamics simulations were performed for the baicalein-ERK1/2 complex to explore potential interaction mechanisms. The root mean square deviation (RMSD) for the ERK1-baicalein and ERK2-baicalein systems ranged from 0.10–2.50 Å and 0.15–2.25 Å (Figure 6F). The root mean square fluctuation
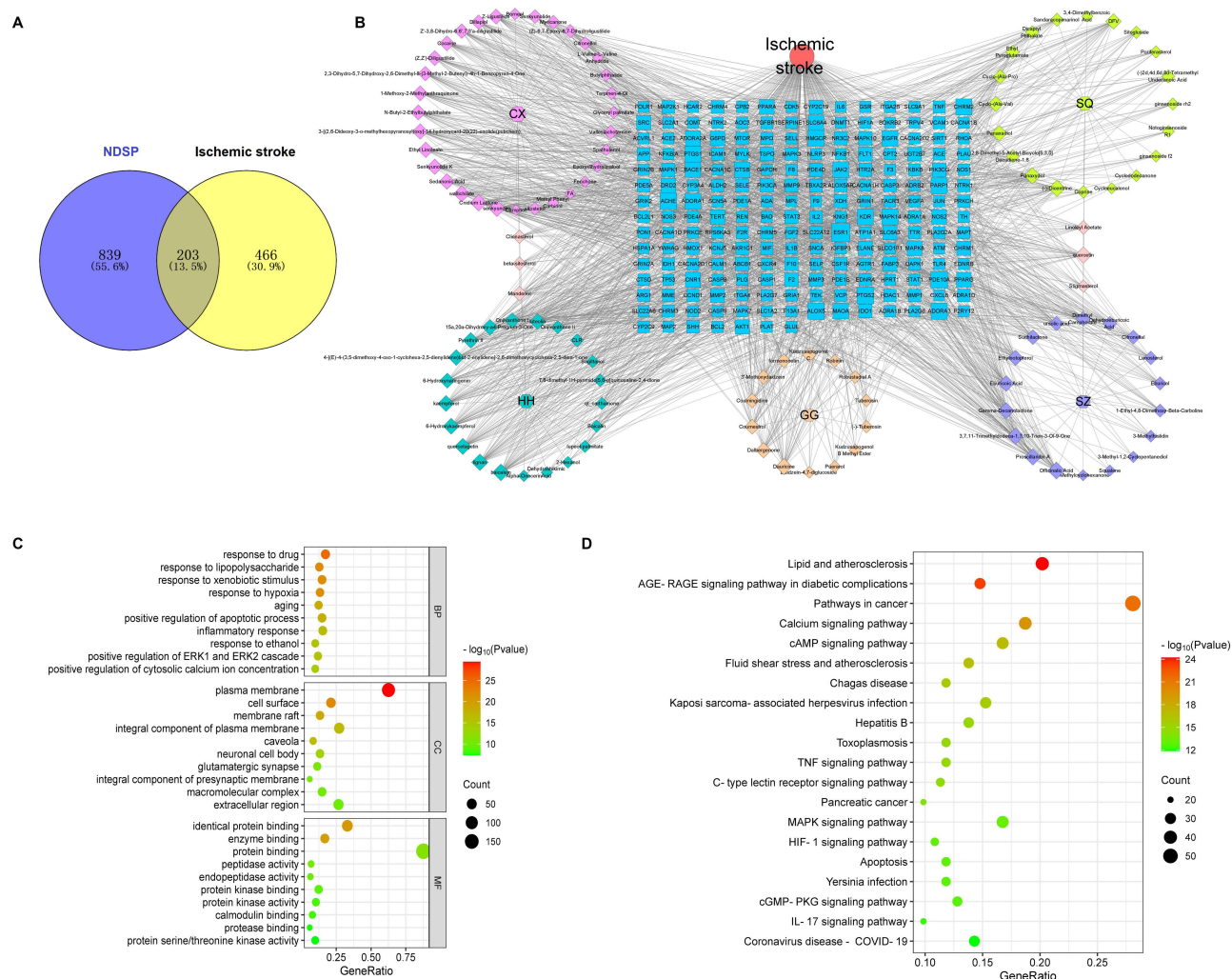
Figure 5 Identified ferroptosis-regulating genes as candidate targets of NDSP activity. (**A**) Venn diagram of the identified common targets of drugs and diseases. (**B**) The Drug-Ingredient-Disease-Target network. (**C**) GO enrichment analysis results. (**D**) KEGG pathway enrichment analysis results.
Abbreviations: NDSP, Naodesheng pills; CX, *Ligusticum chuanxiong* Hort; HH, *Carthamus tinctorius* L; GG, *Pueraria lobata* (Willd.) Ohwi; SZ, *Crataegus pinnatifida* Bunge; SQ, *Panax notoginseng* (Burk.) F.H. Chen.

(RMSF) results indicate that the ERK1/2 protein has good structural rigidity (Figure 6G). The number of hydrogen bonds in the Erk2-baicalein complex remained at approximately three during the molecular dynamics simulations, whereas that in the Erk1-baicalein complex was approximately two (Figure 6H). Thus, the molecular dynamics simulation results were consistent with the molecular docking results showing that ERK1/2-baicalein had a good binding capacity. These findings suggested that NDSP inhibited I/R-induced ferroptosis by modulating the activity of ERK1/2.

Discussion

Several mechanisms, such as oxidative stress, inflammation, glutamate-mediated neuroexcitatory toxicity, and mitochondrial dysfunction, are involved in cerebral I/R injury.[38] Neuronal death is the main cause of neurological and cognitive impairment.[39] Ferroptosis is a type of programmed cell death that plays an important role in pathological conditions, including cancer,[40] cardiovascular disease,[41] diabetes and its associated complications,[9] I/R organ injury,[42–44] as well as numerous neurodegenerative diseases.[8] Increasing evidence shows that ferroptosis is closely related to ischemic stroke.[45,46] In the present study, we assessed the protective effects of NDSP against I/R-induced cerebral ferroptosis

Figure 6 NDSP regulates ferroptosis via the ERK1/2 signaling pathway. (**A**) The constructed PPI network. (**B**) The identified core target. (**C**) Western blot analysis of ERK1/2, p-ERK1/2 protein levels. The β-actin was used as the loading control. (**D**) Representative images of immunohistochemical staining for p-ERK1/2 in the rat cerebral cortex (400× magnification, scale bar: 50 μm). (**E**) Details of the molecular docking analysis of baicalein and ERK1/2. (**F**) Details of the RMSD of baicalein and ERK1/2. (**G**) Details of the RMSF of baicalein and ERK1/2. (**H**) Number of H bonds of baicalein and ERK1/2. Data presented as mean ± SEM (n = 3 independent experiments; statistical analysis performed by bootstrap method; *$P < 0.05$).
Abbreviations: I/R, Ischemia-reperfusion; NDSP, Naodesheng pills; NDSP-L, low-dose NDSP; NDSP-H, high-dose NDSP; OGD/R, Oxygen-glucose deprivation/reoxygenation.

and explored its underlying mechanisms. We demonstrated that pretreatment of rats with NDSP 1.08 g/kg alleviated I/R-induced ferroptosis, decreased infarct area, and improved overall neurological scores.

The regulatory mechanism of ferroptosis involves perturbations in iron transport, amino acid metabolism, and lipid peroxidation.[9] Iron is crucial for normal neuronal function at baseline, and an overabundance of iron is associated with the exacerbation of several neurodegenerative diseases.[47] Regarding the modulation of iron levels, TFR1 and DMT1 are involved in intracellular iron regulation, maintaining iron metabolism and homeostasis. TFR1 facilitates the cellular uptake of Fe^{3+} via endocytosis of transferrin, which is subsequently reduced to Fe^{2+} by the six-transmembrane epithelial antigen protein 3. DMT1 and ZIP8/14 transport Fe^{2+} into the cytoplasm.[48,49] Aberrant expression of TFR1 and DMT1 serves as a marker of ferroptosis. Here, we investigated the effect of NDSP on iron metabolic pathways and found that NDSP attenuated the imbalance in iron metabolism by decreasing TFR1 and DMT1 expression.

The accumulation of iron-dependent lipid peroxidation products is a characteristic feature of ferroptosis. Excessive lipid ROS levels induce oxidative stress, damaging proteins, lipids, nucleic acids, membrane rupture, and subsequent cell death.[50] In this context, the inhibition of ferroptosis presents a potential strategy for ameliorating I/R injury. We observed that in brain tissue samples of I/R-treated rats or OGD/R-treated SH-SY5Y cells, there was a significant surge in the levels of MDA, Fe^{2+}, and H_2O_2 in brain tissue samples from I/R-treated rats. The NDSP treatment reversed these

changes. The SLC7A11/GPX4 signaling axis is a critical pathway that regulates glutathione production.[51] Downregulation of SLC7A11 leads to reduced intracellular cystine levels, depleting glutathione biosynthesis, and indirectly suppressing GPX4 activity, consequently promoting ferroptosis. NDSP treatment restored the expression of SLC7A11 and GPX4, thereby exerting a protective effect against cerebral I/R injury. In contrast, incubation with RSL3, a GPX4 inhibitor, abrogated the protective effects of NDSP against OGD/R-induced ROS generation. These findings suggested that NDSP protects against I/R-induced cerebral injury by inhibiting ferroptosis.

This study used network pharmacology to analyze how NDSP inhibited ferroptosis induced by cerebral ischemia-reperfusion. We identified 203 common targets and performed GO and KEGG for these 203 common targets. GO enrichment analysis suggested that NDSP treatment for I/R-induced injury involves positive regulation of the ERK1 and ERK2 cascades in biological processes, and KEGG enrichment analysis indicated that common targets are involved in the MAPK signaling pathway. Although the MAPK signaling pathway did not rank high in the GO and KEGG analyses, the results of the topology analysis of the PPI network suggested that genes such as *MAPK3, SRC, MAPK1, STAT3, TP53*, and *AKT1* are the core targets of NDSP. These results suggest that ERK1/2 may be involved in the effects of NDSP on I/R-induced ferroptosis.

The MAPK signaling cascade is essential for regulating ferroptosis, as activated ERK1/2 regulates the expression of ferroptosis-related genes. ERK1/2 increases the sensitivity of human breast epithelial cells to ferroptosis, and ERK inhibition upregulated the expression of GPX4.[15] In pancreatic ductal adenocarcinoma, ERK1/2 is required for elastin-induced ferroptosis.[52] In macrophages, ERK1/2-mediated ferritinophagy contributes to ferroptosis induced by cadmium telluride quantum dots.[53] Zille et al demonstrated that the ERK1/2 inhibitor U0126 abrogated hemin-induced ferroptosis in primary cortical neurons.[54] In a spinal cord ischemia/reperfusion injury model, the ERK1/2/c-Myc/TFR1 signaling axis participates in the Eph receptor A4 regulation of motor neuron ferroptosis.[55] Our observations indicated that NDSP alleviated the increase in ERK1/2 phosphorylation mediated by I/R and OGD/R. These results are consistent with those reported by pharmacologists. Based on our molecular docking results, baicalein displayed the most satisfactory binding affinity for ERK1/2 compared to the other identified active ingredients. Furthermore, the molecular dynamics simulation results of baicalein-ERK1/2 supported those of molecular docking. However, further research is needed to explore how the active ingredients of NDSP regulate ERK1/2 phosphorylation.

Conclusion

In summary, we have demonstrated that NDSP exerts a protective effect against ferroptosis during cerebral I/R injury. Furthermore, our findings indicated that this protective mechanism is associated with the inhibition of ERK1/2 phosphorylation. Our study offers valuable insights for potentially improving therapeutic approaches for the treatment of stroke.

Abbreviations

ADME, absorption, distribution, metabolism and excretion; CCA, common carotid artery; DMT1, divalent metal-ion transporter-1; ECA, external carotid artery; ERK1/2, mitogen-activated protein kinase 1/2; GPX4, glutathione peroxidase 4; GSH, glutathione; H_2O_2, hydrogen peroxide; ICA, internal carotid artery; I/R, ischemia/reperfusion; MDA, malondialdehyde; NDSP, Naodesheng pill; NDSP-L, low-dose NDSP; NDSP-H, high-dose NDSP; OGD/R, oxygen glucose deprivation/reoxygenation; OD, optical density; ROS, reactive oxygen species; SEM, standard error of the mean; SLC7A11, solute carrier family 7 member 11; SOD, superoxide dismutase; TCMSP, Traditional Chinese Medicine Systems Pharmacology Database and Analysis Platform; TEM, transmission electron microscopy; TFR1, transferrin receptor 1; TTC, triphenyltetrazolium chloride.

Data Sharing Statement

The datasets used and/or analyzed in the current study are available from the corresponding author (Yong-Yu Yang) upon reasonable request. Uncropped gels and blots are provided in Supplementary Figure 1.

Ethics Approval and Consent to Participate

All experimental protocols were designed according to the Guide for the Care and Use of Laboratory Animals (NIH Publication, 8th edition, 2011) and approved by the Animal Ethics and Welfare Committee of the Second Xiangya Hospital of Central South University (No. 2021955).

Author Contributions

All authors made a significant contribution to the work reported, whether that is in the conception, study design, execution, acquisition of data, analysis, and interpretation, or in all these areas; took part in drafting, revising, or critically reviewing the article; gave final approval of the version to be published; agreed on the journal to which the article has been submitted; and agreed to be accountable for all aspects of the work.

Funding

Disclosure

The authors have no competing interest to declare in this work.

References

1. Jiang C-T, Wu W-F, Deng Y-H, et al. Modulators of microglia activation and polarization in ischemic stroke (Review). *Mol Med Rep*. 2020;21 (5):2006–2018. doi:10.3892/mmr.2020.11003
2. Ren W, Yang X. Pathophysiology of Long Non-coding RNAs in Ischemic Stroke. *Front Mol Neurosci*. 2018;11:96. doi:10.3389/fnmol.2018.00096
3. Naseh M, Vatanparast J, Rafati A, et al. The emerging role of FTY720 as a sphingosine 1-phosphate analog for the treatment of ischemic stroke: the cellular and molecular mechanisms. *Brain Behav*. 2021;11:e02179. doi:10.1002/brb3.2179
4. Xia XH, Li Q, Liu M. Neuroprotective effect of a formula, moschus combined with borneolum synthcticum, from traditional Chinese medicine on ischemia stroke in rats. *Evid Based Complement Alternat Med*. 2014;2014:157938. doi:10.1155/2014/157938
5. Patel AMR, Apaijai N, Chattipakorn N, et al. The protective and reparative role of colony-stimulating factors in the brain with cerebral ischemia/ reperfusion injury. *Neuroendocrinology*. 2021;111:1029–1065. doi:10.1159/000512367
6. Li X, Zhuang X, Qiao T. Role of ferroptosis in the process of acute radiation-induced lung injury in mice. *Biochem Biophys Res Commun*. 2019;519:240–245. doi:10.1016/j.bbrc.2019.08.165
7. Ren JX, Sun X, Yan XL, et al. Ferroptosis in neurological diseases. *Front Cell Neurosci*. 2020;14:218. doi:10.3389/fncel.2020.00218
8. Vitalakumar D, Sharma A, Flora SJS. Ferroptosis: a potential therapeutic target for neurodegenerative diseases. *J Biochem Mol Toxicol*. 2021;35: e22830. doi:10.1002/jbt.22830
9. Yang XD, Yang YY. Ferroptosis as a novel therapeutic target for diabetes and its complications. *Front Endocrinol*. 2022;13:853822. doi:10.3389/ fendo.2022.853822
10. Guan X, Li Z, Zhu S, et al. Galangin attenuated cerebral ischemia-reperfusion injury by inhibition of ferroptosis through activating the SLC7A11/ GPX4 axis in gerbils. *Life Sci*. 2021;264:118660. doi:10.1016/j.lfs.2020.118660
11. Patt A, Horesh IR, Berger EM, et al. Iron depletion or chelation reduces ischemia/reperfusion-induced edema in gerbil brains. *J Pediatr Surg*. 1990;25:224–227; discussion 227–228. doi:10.1016/0022-3468(90)90407-z
12. Liu P, Yang X, Niu J, et al. Hyperglycemia aggravates ischemic brain damage via ERK1/2 activated cell autophagy and mitochondrial fission. *Front Endocrinol*. 2022;13:928591. doi:10.3389/fendo.2022.928591
13. Alessandrini A, Namura S, Moskowitz MA, et al. MEK1 protein kinase inhibition protects against damage resulting from focal cerebral ischemia. *Proc Natl Acad Sci U S A*. 1999;96:12866–12869. doi:10.1073/pnas.96.22.12866
14. Su L, Jiang X, Yang C, et al. Pannexin 1 mediates ferroptosis that contributes to renal ischemia/reperfusion injury. *J Biol Chem*. 2019;294:19395–19404. doi:10.1074/jbc.RA119.010949
15. Poursaitidis I, Wang X, Crighton T, et al. Oncogene-selective sensitivity to synchronous cell death following modulation of the amino acid nutrient cystine. *Cell Rep*. 2017;18:2547–2556. doi:10.1016/j.celrep.2017.02.054
16. Luo L, Kang J, Zhao W, et al. Validated LC-MS/MS method for simultaneous quantification of seven components of Naodesheng in rat serum after oral administration and its application to a pharmacokinetic study. *J Pharm Biomed Anal*. 2019;174:1–7. doi:10.1016/j.jpba.2019.05.036
17. Yu Z, Gao X, Zhao Y, et al. Simultaneous determination of components in preparation Naodesheng injection by high performance liquid chromatograph-atmospheric pressure chemical ionization mass spectrometry (HPLC-MS/APCI). *Chem Pharm Bull*. 2006;54:588–590. doi:10.1248/ cpb.54.588
18. Yu Z, Gao X, Zhao Y, et al. Determination of safflor yellow A, puerarin, ferulic acid, ginsenoside Rg1, and Rb1 in the Traditional Chinese Medicinal preparation Naodesheng injection by high-performance liquid chromatography. *J Chromatogr Sci*. 2006;44:272–275. doi:10.1093/chromsci/44.5.272
19. Luo L, Kang J, He Q, et al. A NMR-based metabolomics approach to determine protective effect of a combination of multiple components derived from naodesheng on ischemic stroke rats. *Molecules*. 2019;24:1831. doi:10.3390/molecules24091831
20. Zhang B, Zhao J, Guo P, et al. Effects of Naodesheng tablets on amyloid beta-induced dysfunction: a traditional Chinese herbal formula with novel therapeutic potential in *Alzheimer*'s disease revealed by systems pharmacology. *Biomed Pharmacother*. 2021;141:111916. doi:10.1016/j.biopha.2021.111916
21. Feng XF, Li MC, Lin ZY, et al. Tetramethylpyrazine promotes stroke recovery by inducing the restoration of neurovascular unit and transformation of A1/A2 reactive astrocytes. *Front Cell Neurosci*. 2023;17:1125412. doi:10.3389/fncel.2023.1125412

22. Yu L, Jin Z, Li M, et al. Protective potential of hydroxysafflor yellow A in cerebral ischemia and reperfusion injury: an overview of evidence from experimental studies. *Front Pharmacol*. 2022;13:1063035. doi:10.3389/fphar.2022.1063035

23. Liu B, Tan Y, Wang D, et al. Puerarin for ischaemic stroke. *Cochrane Database Syst Rev*. 2016;2:Cd004955. doi:10.1002/14651858.CD004955.pub3

24. Ou L, Li J, Wang R, et al. Effects of different extracting techniques on Naodesheng against focal cerebral infarction of rats. *Chinese Traditional and Herbal Drugs*. 2005;36:393–395.

25. Zhang L, Cheng XR, Chen RY, et al. Protective effect of effective composite of Chinese medicine prescription naodesheng against focal cerebral ischemia in rats. *Chin J Integr Med*. 2009;15:377–383. doi:10.1007/s11655-009-0377-4

26. Luo L, Zhen L, Xu Y, et al. (1)H NMR-based metabolomics revealed protective effect of Naodesheng bioactive extract on ischemic stroke rats. *J Ethnopharmacol*. 2016;186:257–269. doi:10.1016/j.jep.2016.03.059

27. Zuo X, Li Q, Ya F, et al. Ginsenosides Rb2 and Rd2 isolated from Panax notoginseng flowers attenuate platelet function through P2Y(12)-mediated cAMP/PKA and PI3K/Akt/Erk1/2 signaling. *Food Funct*. 2021;12:5793–5805. doi:10.1039/d1fo00531f

28. Yang F, Li J, Zhu J, et al. Hydroxysafflor yellow A inhibits angiogenesis of hepatocellular carcinoma via blocking ERK/MAPK and NF-κB signaling pathway in H22 tumor-bearing mice. *Eur J Pharmacol*. 2015;754:105–114. doi:10.1016/j.ejphar.2015.02.015

29. Wang Y, Zhen Y, Wu X, et al. Vitexin protects brain against ischemia/reperfusion injury via modulating mitogen-activated protein kinase and apoptosis signaling in mice. *Phytomedicine*. 2015;22:379–384. doi:10.1016/j.phymed.2015.01.009

30. Kang Z, Xiao Q, Wang L, et al. The combination of astragaloside IV and Panax notoginseng saponins attenuates cerebral ischaemia-reperfusion injury in rats through ferroptosis and inflammation inhibition via activating Nrf2. *J Pharm Pharmacol*. 2023;75:666–676. doi:10.1093/jpp/rgad011

31. Li C, Liu Y. Puerarin reduces cell damage from cerebral ischemia-reperfusion by inhibiting ferroptosis. *Biochem Biophys Res Commun*. 2024;693:149324. doi:10.1016/j.bbrc.2023.149324

32. Lou T, Wu H, Feng M, et al. Integration of metabolomics and transcriptomics reveals that Da Chuanxiong Formula improves vascular cognitive impairment via ACSL4/GPX4 mediated ferroptosis. *J Ethnopharmacol*. 2024;325:117868. doi:10.1016/j.jep.2024.117868

33. Arifin WN, Zahiruddin WM. Sample size calculation in animal studies using resource equation approach. *Malays J Med Sci*. 2017;24:101–105. doi:10.21315/mjms2017.24.5.11

34. Zhu F, Chen H, Xu M, et al. Cryptotanshinone possesses therapeutic effects on ischaemic stroke through regulating STAT5 in a rat model. *Pharm Biol*. 2021;59:465–471. doi:10.1080/13880209.2021.1914672

35. Wang L, Zhao H, Zhai ZZ, et al. Protective effect and mechanism of ginsenoside Rg1 in cerebral ischaemia-reperfusion injury in mice. *Biomed Pharmacother*. 2018;99:876–882. doi:10.1016/j.biopha.2018.01.136

36. Yang RX, Lei J, Wang BD, et al. Pretreatment with sodium phenylbutyrate alleviates cerebral ischemia/reperfusion injury by upregulating DJ-1 protein. *Front Neurol*. 2017;8:256. doi:10.3389/fneur.2017.00256

37. Yang M, Li X, Li H, et al. Baicalein inhibits RLS3-induced ferroptosis in melanocytes. *Biochem Biophys Res Commun*. 2021;561:65–72. doi:10.1016/j.bbrc.2021.05.010

38. Wu D, Wang J, Wang H, et al. Protective roles of bioactive peptides during ischemia-reperfusion injury: from bench to bedside. *Life Sci*. 2017;180:83–92. doi:10.1016/j.lfs.2017.05.014

39. Singh V, Mishra VN, Chaurasia RN, et al. Modes of calcium regulation in ischemic neuron. *Indian J Clin Biochem*. 2019;34:246–253. doi:10.1007/s12291-019-00838-9

40. Wang Y, Wei Z, Pan K, et al. The function and mechanism of ferroptosis in cancer. *Apoptosis*. 2020;25:786–798. doi:10.1007/s10495-020-01638-w

41. Chen Z, Yan Y, Qi C, et al. The role of ferroptosis in cardiovascular disease and its therapeutic significance. *Front Cardiovasc Med*. 2021;8:733229. doi:10.3389/fcvm.2021.733229

42. Lillo-Moya J, Rojas-Solé C, Muñoz-Salamanca D, et al. Targeting ferroptosis against ischemia/reperfusion cardiac injury. *Antioxidants*. 2021;10:667. doi:10.3390/antiox10050667

43. Tao WH, Shan XS, Zhang JX, et al. Dexmedetomidine attenuates ferroptosis-mediated renal ischemia/reperfusion injury and inflammation by inhibiting ACSL4 via α2-AR. *Front Pharmacol*. 2022;13:782466. doi:10.3389/fphar.2022.782466

44. Ye J, Peng J, Liu K, et al. MCTR1 inhibits ferroptosis by promoting Nrf2 expression to attenuate hepatic ischemia-reperfusion injury. *Am J Physiol Gastrointest Liver Physiol*. 2022;323:G283–G293. doi:10.1152/ajpgi.00354.2021

45. Tuo QZ, Lei P, Jackman KA, et al. Tau-mediated iron export prevents ferroptotic damage after ischemic stroke. *Mol Psychiatry*. 2017;22:1520–1530. doi:10.1038/mp.2017.171

46. Wang P, Cui Y, Ren Q, et al. Mitochondrial ferritin attenuates cerebral ischaemia/reperfusion injury by inhibiting ferroptosis. *Cell Death Dis*. 2021;12:447. doi:10.1038/s41419-021-03725-5

47. Reichert CO, de Freitas FA, Sampaio-Silva J, et al. Ferroptosis mechanisms involved in neurodegenerative diseases. *Int J Mol Sci*. 2020;21:8765. doi:10.3390/ijms21228765

48. Sendamarai AK, Ohgami RS, Fleming MD, et al. Structure of the membrane proximal oxidoreductase domain of human Steap3, the dominant ferrireductase of the erythroid transferrin cycle. *Proc Natl Acad Sci U S A*. 2008;105:7410–7415. doi:10.1073/pnas.0801318105

49. Powers M, Minchella D, Gonzalez-Acevedo M, et al. Loss of hepatic manganese transporter ZIP8 disrupts serum transferrin glycosylation and the glutamate-glutamine cycle. *J Trace Elem Med Biol*. 2023;78:127184. doi:10.1016/j.jtemb.2023.127184

50. Ying JF, Lu ZB, Fu LQ, et al. The role of iron homeostasis and iron-mediated ROS in cancer. *Am J Cancer Res*. 2021;11:1895–1912.

51. Yuan Y, Zhai Y, Chen J, et al. Kaempferol ameliorates oxygen-glucose deprivation/reoxygenation-induced neuronal ferroptosis by activating Nrf2/SLC7A11/GPX4 axis. *Biomolecules*. 2021;11:923. doi:10.3390/biom11070923

52. Gao H, Bai Y, Jia Y, et al. Ferroptosis is a lysosomal cell death process. *Biochem Biophys Res Commun*. 2018;503:1550–1556. doi:10.1016/j.bbrc.2018.07.078

53. Liu N, Liang Y, Wei T, et al. The role of ferroptosis mediated by NRF2/ERK-regulated ferritinophagy in CdTe QDs-induced inflammation in macrophage. *J Hazard Mater*. 2022;436:129043. doi:10.1016/j.jhazmat.2022.129043

54. Zille M, Karuppagounder SS, Chen Y, et al. Neuronal death after hemorrhagic stroke in vitro and in vivo shares features of ferroptosis and necroptosis. *Stroke*. 2017;48:1033–1043. doi:10.1161/strokeaha.116.015609

55. Dong Y, Ai C, Chen Y, et al. Eph receptor A4 regulates motor neuron ferroptosis in spinal cord ischemia/reperfusion injury in rats. *Neural Regen Res*. 2023;18:2219–2228. doi:10.4103/1673-5374.369118